RESEARCH ARTICLE

Energy & Environmental Materials WILEY

Superior Electrocatalyst

Mo_2P Monolayer as a Superior Electrocatalyst for Urea Synthesis from Nitrogen and Carbon Dioxide Fixation: A Computational Study

Dongxu Jiao, Zhongxu Wang, Yuejie Liu, Qinghai Cai, Jingxiang Zhao*, Carlos R. Cabrera, and Zhongfang Chen**

Urea synthesis through the simultaneous electrocatalytic reduction of N_2 and CO_2 molecules under ambient conditions holds great promises as a sustainable alternative to its industrial production, in which the development of stable, highly efficient, and highly selective catalysts to boost the chemisorption, activation, and coupling of inert N_2 and CO_2 molecules remains rather challenging. Herein, by means of density functional theory computations, we proposed a new class of two-dimensional nanomaterials, namely, transition-metal phosphide monolayers (TM_2P, TM = Ti, Fe, Zr, Mo, and W), as the potential electrocatalysts for urea production. Our results showed that these TM_2P materials exhibit outstanding stability and excellent metallic properties. Interestingly, the Mo_2P monolayer was screened out as the best catalyst for urea synthesis due to its small kinetic energy barrier (0.35 eV) for C–N coupling, low limiting potential (−0.39 V), and significant suppressing effects on the competing side reactions. The outstanding catalytic activity of the Mo_2P monolayer can be ascribed to its optimal adsorption strength with the key *NCON species due to its moderate positive charges on the Mo active sites. Our findings not only propose a novel catalyst with high-efficiency and high-selectivity for urea production but also further widen the potential applications of metal phosphides in electrocatalysis.

1. Introduction

Urea is the fertilizer with the highest nitrogen content, contributing significantly to global agricultural growth and ensuring the survival of most of the world's population.[1–3] At present, the world production of urea is about 100 million tons $year^{-1}$, which mainly comes from the reaction of CO_2 and NH_3 under high temperature and pressure conditions (at temperature of 150–200 °C and pressure of 150–250 bar).[4] As matters stand, the main source of NH_3 comes from the conventional Haber–Bosch method, which also requires drastic reaction conditions, leading to a consumption of about 2% of the global energy.[5,6] As a result, fossil fuels will be heavily consumed and cause serious damage to the environment. To this end, the search for a green and sustainable urea synthesis under ambient conditions is essential for the development of human society.

Compared with huge energy consumption in the current industrial processes, the electrochemical urea synthesis by the direct reaction between N_2 and CO_2 under milder conditions has emerged as a more attractive alternative approach ($N_2 + CO_2 + 6H^+ \rightarrow CO(NH_2)_2 + H_2O$).[7,8] However, most electrocatalysts show low activity during urea synthesis progress due to the difficulty of activating N_2 and CO_2 molecules and the sluggish C–N coupling. In addition, the complex product distribution and non-negligible competing reactions, especially nitrogen reduction reaction (NRR) and hydrogen evolution reaction (HER), also lead to the selectivity problem in this process.[9,10] Therefore, further developing high-performance electrocatalysts to overcome the above challenges is an urgent task to advance efficient and environmentally benign urea production.

Remarkably, in a pioneering work, Chen et al.[11] fabricated the Pd–Cu alloy nanoparticles on TiO_2 nanosheets as an electrocatalyst and demonstrated that urea could be produced via direct coupling of N_2 and CO_2 molecules in water under ambient conditions. Moreover, Zhang's group successfully synthesized $BiFeO_3/BiVO_4$[12] and $Bi–BiVO_4$[13] heterostructures to promote urea formation by accelerating local charge redistribution, while inhibiting CO poisoning and improving selectivity. They also designed unique frustrated Lewis pairs in InOOH[14] and $Ni_3(BO_3)_2$[15] to enhance the adsorption ability of

Dr. D. Jiao, Dr. Z. Wang, Prof. Q. Cai, Prof. J. Zhao
College of Chemistry and Chemical Engineering, and Key Laboratory of Photonic and Electronic Bandgap Materials, Ministry of Education, Harbin Normal University, Harbin 150025, China
E-mail: xjz_hmily@163.com
Dr. Y. Liu
Modern Experiment Center, Harbin Normal University, Harbin 150025, China
E-mail: liuyuejie@hrbnu.edu.cn
Prof. Q. Cai
Heilongjiang Province Collaborative Innovation Center of Cold Region Ecological Safety, Harbin 150025, China
Prof. C. R. Cabrera
Department of Chemistry and Biochemistry, The University of Texas at El Paso, El Paso TX 79968, USA
Prof. Z. Chen
Department of Chemistry, University of Puerto Rico, Rio Piedras Campus, San Juan, Puerto Rico 00931, USA
E-mail: zhongfangchen@gmail.com
The ORCID identification number(s) for the author(s) of this article can be found under https://doi.org/10.1002/eem2.12496.

DOI: 10.1002/eem2.12496

N_2 and CO_2, and thus improve the catalytic performance for urea synthesis. Nevertheless, the bulk materials-based catalysts usually suffer from their limited and ambiguous active sites. Thus, further designing highly active and selective electrocatalysts with uniform, specific, and abundant active sites that can simultaneously capture and activate N_2 and CO_2 to form urea is highly crucial.

Compared with other nanomaterials, two-dimensional (2D) nanomaterials exhibit even more outstanding properties, such as larger specific surface area and more abundant active sites, thus endowing them as promising catalysts for many important electrocatalytic reactions, such as oxygen reduction/evolution reactions (ORR/OER), HER, CO_2 reduction reaction (CO_2RR), and NRR.[16–19] Among various 2D nanomaterials, transition metal phosphides (TMPs) are of particular interest in electrocatalysis due to their abundant structures and excellent catalytic performance.[20–30] For example, Zhu et al.[25] reported that the fabricated MoP_2 nanosheet shows exceptionally high catalytic activity toward HER. Yang et al.[20] successfully synthesized 2D Co_2P nanomaterials to effectively catalyze OER. Theoretically, Lou et al.[26] identified a novel Mo_2P_3 monolayer with a Janus structure as electrocatalyst for HER, while our most recent theoretical study suggested that the as-designed Pt_2P_3 monolayer can serve as a promising bifunctional catalyst for HER and CO_2RR.[27]

Although 2D nanomaterials possess outstanding properties and wide applications in electrocatalysis, good catalytic performance for urea synthesis has been revealed in only a few 2D materials, namely, MBenes,[31] CuB_{12},[32] and Si-doped graphitic carbon nitride (g-C_6N_6) sheet.[33] Thus, very likely other 2D nanomaterials have potential as electrocatalysts in the urea industry but escaped our attention so far. With diverse structures and excellent properties, 2D TMP materials came up as the top candidates for our exploration.

Herein, by means of comprehensive density functional theory (DFT) computations, we systematically studied the catalytic performance of a new kind of 2D transition metal phosphides (TM_2P, TM = Ti, Fe, Zr, Mo, and W) monolayers with rich exposed metal atoms on their basal plane for urea electrosynthesis. We found that N_2 and CO_2 molecules can be simultaneously chemisorbed on TM_2P surfaces. Surprisingly, the sufficiently activated N_2 and CO_2 can be easily coupled on the Mo_2P monolayer to form a key *NCON intermediate with a rather low kinetic barrier of 0.35 eV, which can be further hydrogenated to urea production with a small limiting potential of −0.39 V along an alternative mechanism. More importantly, the catalytic trends of these TM_2P candidates are highly related to their adsorption strength with *NCON species, which can be explained by the remarkable difference in the positive charges of the exposed metal-active sites. Thus, the 2D Mo_2P monolayer is expected to be a high-performance electrocatalyst for urea synthesis.

2. Computational Models and Methods

Our spin-polarized DFT calculations were performed with the plane-wave basis set as implemented in the Vienna Ab Initio Simulation Package (VASP).[34,35] The projector-augmented wave potential was employed to describe the interactions between electrons and ions.[36,37] The exchange–correlation interactions were determined by the Perdew–Burke–Ernzerhof functional within the generalized gradient approximation,[38] and a cutoff energy of 550 eV was adopted for the plane-wave basis set. The convergence criteria for the residual force and the energy on each atom during structure were set to 0.03 eV $Å^{-1}$ and 10^{-5} eV, respectively. The empirical correction in Grimme's method (DFT + D3) was used to describe the van der Waals interactions.[39] The climbing image nudged elastic band (CI-NEB) method was utilized to locate the involved transition states.[40] The adsorption energy (E_{ads}) of adsorbed species on the catalyst surface was defined as $E_{ads} = E_{total} - E_{adsorbate} - E_{catalyst}$, in which the E_{total}, $E_{adsorbate}$, and $E_{surface}$ represent the total energies of adsorbed species on the catalyst, isolated adsorbate, and catalyst, respectively. According to this definition, a more negative E_{ads} represents a stronger interaction between adsorbate and catalyst.

TM_2P-based catalysts were built using a 5 × 5 supercell, in which a vacuum space of 15 Å in the z-direction was employed to avoid the interactions between adjacent periodic images. A 3 × 3 × 1 Monkhorst–Pack k-point mesh was adopted to sample the 2D Brillouin zone for structure optimizations, while a denser 15 × 15 × 1 k-point was used for electronic property computations. The band structures were computed by the Heyd–Scuseria–Ernzerhof hybrid functional.[41,42] Ab initio molecular dynamics (AIMD) simulations using the NVT ensemble[43] were carried out to evaluate the environmental stability of Mo_2P materials. The phonon spectra were computed to assess their kinetic stability based on the density functional perturbation theory using Phonopy code.[44] The change in the Gibbs free energy change (ΔG) for each possible step during the electrochemical synthesis of urea was obtained using the computational hydrogen electrode model,[45,46] and further details on the computations of free energy diagrams and limiting potentials are given in the Supporting Information.

3. Results and Discussion

3.1. Structures, Stabilities, and Properties of TM_2P Monolayer

Figure 1 presents the schematic structure of a 2D TM_2P monolayer, and the corresponding structural parameters are summarized in Table S1, Supporting Information. Clearly, there are two metal and one P atoms in the unit cell of a TM_2P monolayer, forming a three-atom-thick layer with a sandwich structure, in which the metal atoms are exposed on the outmost layers. Interestingly, each metal atom on the basal plane of the TM_2P monolayer binds with three P atoms, thus exhibiting a low coordination number, which is conducive to chemosorbing and activating the inert N_2 and CO_2 molecules. Furthermore, according to the computed electronic band structures (Figure S1, Supporting Information), all the five TM_2P monolayers examined here have several bands across the Fermi level (E_F), thus are metallic and have excellent electronic conductivity. Note that the above results are well consistent with previous theoretical investigations.[47–50]

The stability of a given catalyst is always an unavoidable issue for its practical application. To this end, we evaluated the thermodynamic, dynamic, and mechanical stabilities of these TM_2P catalysts. Thermodynamically, the cohesive energies of the Ti_2P, Fe_2P, Zr_2P, Mo_2P, and W_2P monolayers are computed to be 5.02, 4.53, 5.28, 5.38, and 6.15 eV $atom^{-1}$ (Table S1, Supporting Information), respectively, which are comparable (even higher) to those of some well-established 2D nanomaterials, such as phosphorene (3.30 eV $atom^{-1}$),[51] Fe_2Si (4.32 eV $atom^{-1}$),[52] and FeP_3 (4.13 eV $atom^{-1}$),[1-5,10,13] suggesting their good thermodynamic stability. Dynamically, the phonon spectra of these TM_2P-based materials were examined (Figure S2, Supporting Information), and no imaginary phonon modes were found in their entire Brillouin zones, thus indicating their good kinetic stability.

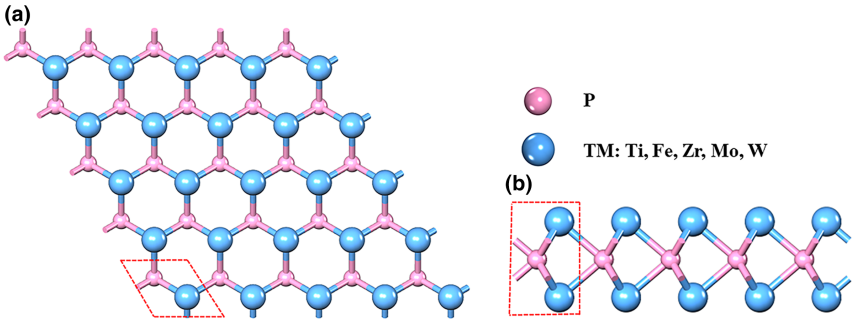

Figure 1. a) Top and b) side views of the schematic structure of TM_2P monolayer. The red-dashed lines represent a unit cell of the TM_2P monolayer.

Additionally, their computed elastic constants (Table S2, Supporting Information) well satisfy the Born criteria ($C_{11}C_{22} - C_{12}^2 > 0$; $C_{66} > 0$),[53] implying their excellent mechanical stability.

An important advantage of 2D nanomaterials in catalysis is their abundant active sites. We thus evaluated the density of active sites (ρ_{AS}) of these TM_2P monolayers, which can be determined by the total number of active sites per unit area. The computed ρ_{AS} values are in the range from 1.50×10^{15} to 2.53×10^{15} site cm^{-2} (Table S1, Supporting Information), which is much higher than those of Ti_2CO_2 (1.30×10^{15} site cm^{-2}),[54] Mo_2C (1.39×10^{15} site cm^{-2}),[55] MoS_2 base (1.14×10^{15} site cm^{-2}),[56] Mo_3P_2 (1.09×10^{15} site cm^{-2}),[26] and FeP_3 (6.72×10^{14} site cm^{-2}),[30] suggesting their rather abundant active sites. Furthermore, there is an obvious charge transfer from metal to P atoms, resulting in the significant accumulation of positive charge on the exposed metal atoms (Table S1, Supporting Information), which may be also beneficial for the capture and activation of inert N_2 and CO_2 reactants.

3.2. Catalytic Performance of TM_2P Monolayer Toward Urea Production

After confirming the unique geometrical structures, excellent stability, inherent metallicity, and abundant active sites, we further explored the catalytic performance of these TM_2P monolayers for urea synthesis. Note that the reduction of N_2 and CO_2 in the aqueous solution to produce urea is a quite complicated process[32] and involves various reaction intermediates (**Figure 2**). Roughly the whole process of urea synthesis can be divided into three stages: 1) strong co-adsorption of N_2 and CO_2 molecules, which is a prerequisite for urea formation; 2) coupling reaction of C–N bond; and 3) hydrogenation of the coupled intermediate. Meanwhile, three main competing reactions, including NRR, CO_2RR, and HER, should be significantly suppressed to ensure the high selectivity of catalysts toward urea production.

Thus, we first examined the adsorption of N_2 and CO_2 molecules on the basal planes of these TM_2P monolayers, in which the Mo_2P monolayer was chosen as a representative for detailed discussions. For the N_2 adsorption, both end-on and side-on configurations were considered. We found that thermodynamically the N_2 molecule prefers being adsorbed on the bridge sites of three Mo atoms via the side-on pattern, in which each N atom bind with three adjacent Mo atoms, leading to the formation of five Mo–N bonds with the lengths of 2.10–2.24 Å (**Figure 3a**), and the computed adsorption energy (ΔE_{ads}) of N_2 molecule is −1.99 eV, which is more negative than that of the end-on pattern (−1.34 eV, Figure S3, Supporting Information). After considering zero-point energy and entropy contributions (Table S3, Supporting Information), the free energy change (ΔG) for N_2 adsorption turns into −1.37 eV, suggesting strong N_2 chemisorption (denoted as $*N_2$), which is also reflected by the obviously elongated N–N bond length (1.31 Å for $*N_2$ vs 1.10 Å for free N_2). Then, the co-adsorption of CO_2 and N_2 molecules on the Mo_2P monolayer was explored, which could greatly affect the subsequent C–N coupling. After considering different possible initial configurations (Figure S4, Supporting Information), we found that CO_2 is preferable to be chemisorbed on the bridge site adjacent to the $*N_2$ species with the ΔE_{ads} of −1.23 eV. In this configuration, both C and O atoms of $*CO_2$ bind with Mo active sites (Figure 3b), and the O–C–O bond angle is bent by about 47°. Thus, two inert reactants, N_2 and CO_2, can be simultaneously chemisorbed on the Mo_2P monolayer, leading to their sufficient activation as revealed by the computed projected density of states due to the strong hybridization between each other (Figure 3c). Notably, similar strong adsorption of N_2 and CO_2 molecules can be observed on other TM_2P materials (Figure S5, Supporting Information).

Following the strong chemisorption of N_2 and CO_2 molecules and the formation of the ($*N_2$ + $*CO_2$) intermediate on the Mo_2P monolayer, we explored the feasibility of the hydrogenation of ($*N_2$ + $*CO_2$). Noteworthy, after one proton-coupled electron transfer step, the intermediate $*N_2H$ + $*CO_2$ or $*N_2$ + *COOH will be formed. Interestingly, $*CO_2$ prefers being hydrogenated to form *COOH with a ΔG of −0.31 eV, which is much lower than that of $*N_2$ to $*N_2H$ (ΔG = 0.35 eV, Table S4, Supporting Information). Notably, though CO_2* could be more easily reduced to *OCHO thermodynamically due to its more negative ΔG (−1.15 eV for *OCHO vs −0.31 eV for *COOH), the kinetic barrier to form *OCHO (1.25 eV) is much higher than that of *COOH formation (0.66 eV). Thus, the formation of the $*N_2$ + *COOH intermediate is more favorable from a kinetic perspective. Subsequently, the

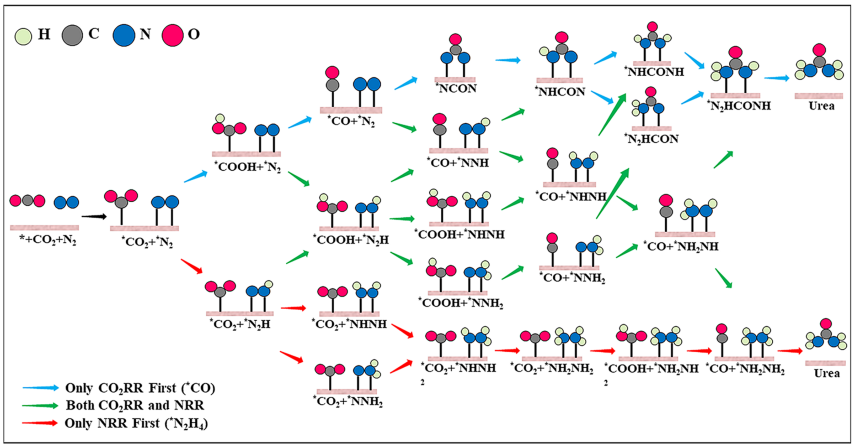

Figure 2. Schematic depiction of all possible pathways for electrocatalytic urea synthesis.

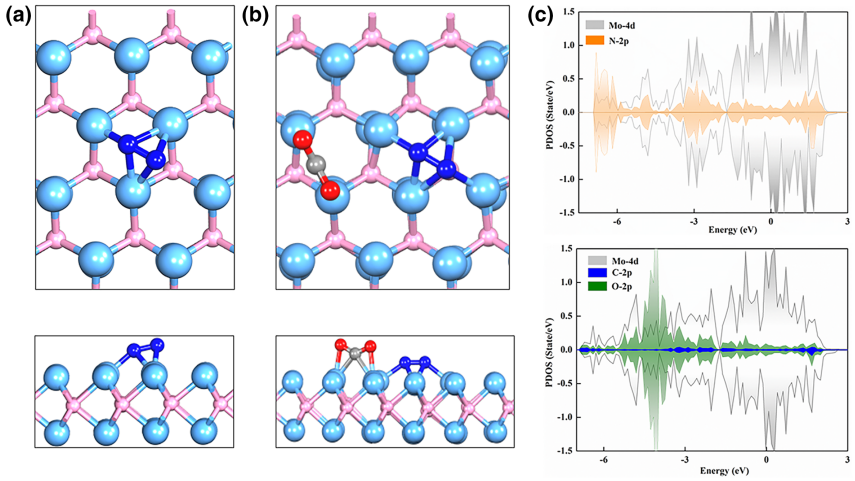

Figure 3. Optimized structures of a) N_2 and b) N_2/CO_2 adsorption on the Mo_2P monolayer; c) the computed projected density of states (PDOS) of the N- and C-2p orbitals in the co-adsorbed N_2/CO_2 species with Mo-4d orbitals of Mo_2P catalyst.

hydrogenation process that occurs on *COOH leads to *CO formation, as its ΔG value (−0.24 eV) is much lower than that of the competing $*N_2H$ formation from $*N_2$ (ΔG = 1.44 eV). Furthermore, the E_{ads} of *CO species on the Mo_2P monolayer (−1.88 eV) is much more negative than the criterion for CO release (−0.98 eV),[57] which suggests that the formed *CO is unlikely to desorb from Mo_2P surface, thus a potential CO poisoning.

The concern of CO poisoning was relieved by our further analysis. Inspired by the recent finding by Li's group[31] that the formation of a tower-like *NCON intermediate is a crucial step for urea production, we explored the reaction pathway involving the formation of *NCON intermediate on the Mo_2P monolayer via the C–N coupling reaction (Figure S6, Supporting Information). According to our computational results, thermodynamically, the reaction of $*N_2 + *CO \rightarrow *NCON$ on the Mo_2P monolayer is more favorable due to its more negative ΔG value (−0.08 eV) than other competing hydrogenation steps, including the formation of $*N_2H + *CO$ (ΔG = 0.33 eV), $*N_2 + *COH$ (ΔG = 2.30 eV), and $*N_2 + *HCO$ (ΔG = 0.63 eV). More interestingly, the C–N coupling between *CO and $*N_2$ on the Mo_2P monolayer only needs to overcome a record low barrier of 0.35 eV (Figure S6, Supporting Information), which is much smaller than all the reported catalysts, including CuB_{12} (0.54 eV),[32] Mo_2B_2 (0.58 eV),[31] Pd–Cu catalysts (0.79 eV),[11] and CuPc NTs (1.67 eV),[58] suggesting its excellent performance for C–N coupling reaction from a kinetic perspective. For comparison, as shown in Figure S7, Supporting Information, the energy barriers for the hydrogenation of $*N_2 + *CO$ to $*N_2H + *CO$, $*N_2 + *COH$, and $*N_2 + *HCO$ are computed to be 1.34, 1.67, and 0.85 eV, respectively, which are much higher than that of *NCON (0.35 eV), suggesting that the C–N coupling reaction is more favorable both thermodynamically and kinetically.

After confirming the formation of the key *NCON intermediate by C–N coupling reaction between $*N_2$ and *CO, we investigated its further hydrogenation on the Mo_2P monolayer. It is found that energetically *NCON is favorably hydrogenated to *NCONH with the ΔG of −0.20 eV, whereas the formation of *NCOHN is endothermic by 0.21 eV (Table S4, Supporting Information) in the free energy diagram. As the next step, *NCONH prefers to be hydrogenated along an alternative pathway to form *NHCONH with the ΔG value of 0.39 eV, which is slightly lower than those of *NCOHNH (ΔG = 0.49 eV) and $*NCONH_2$ (ΔG = 0.51 eV). Furthermore, *NHCONH can be hydrogenated to $*NHCONH_2$ and $*NH_2CONH_2$ with the ΔG values of 0.32 and −0.30 eV, respectively. Finally, the formed urea will be desorbed from the Mo_2P surface. Remarkably, the adsorption energy of urea on the Mo_2P monolayer is −1.70 eV, which is comparable to that of the experimentally available Pd–Cu catalyst (−1.68 eV),[11] suggesting that the desorption process of urea is easily accessible, especially when electrochemical reactions occur in flow cells,[11,31] and thus leading to the recovery of the active sites within the Mo_2P monolayer for the next catalytic cycle.

Since urea electrosynthesis proceeds in aqueous solution, we also evaluated the solvent effect on the catalytic activity of the Mo_2P monolayer for urea formation. To this end, an implicit solvation model in VASPsol was employed with the dielectric constant of 80 for water.[59] By comparing the computed ΔG values of all the elementary steps of urea synthesis with and without solvent effects (Table S5, Supporting Information), we found that these reaction intermediates are actually stabilized (such as $*N_2 + *COOH$, $*N_2 + *CO$, and *NCON) or destabilized (such as *NCONH, *NHCONH, and $*NH_2CONH$) to different degrees. However, the change in the limiting potential for urea formation on the Mo_2P catalyst is only 0.04 V (Figure S8, Supporting Information), suggesting that its excellent catalytic performance is almost unaffected by the solvent effect.

In electrocatalysis, kinetics is also critical in determining the performance of a given catalyst.[60,61] Based on the aforementioned results, we computed the kinetic barriers of all the elementary steps for urea formation on the Mo_2P monolayer. As shown in Figure S9, Supporting Information, the rate-determining step (RDS) for urea synthesis on Mo_2P monolayer is the hydrogenation of *NCONH with a barrier of 1.31 eV, which is lower than that of the experimentally reported CuPc NTs (1.86 eV) with a high yield (143.47 $\mu g\ h^{-1}\ mg_{cat}^{-1}$) and faradaic efficiency (12.99%).[58] Thus, we expected that our proposed Mo_2P monolayer can be utilized as a promising electrocatalyst for urea synthesis from a kinetic perspective.

Overall, the preferred pathway of urea production on the Mo_2P monolayer by the reduction of N_2 and CO_2 can be summarized as $N_2 + CO_2 \rightarrow *N_2 + *CO_2 \rightarrow *N_2 + *COOH \rightarrow *N_2 + *CO \rightarrow$ *NCON → *NCONH → *NHCONH → $*NHCONH_2$ → $*NH_2CONH_2$ (**Figure 4**), in which the step of *NCONH → *NHCONH was identified as the potential-limiting step due to its maximum ΔG value (ΔG_{max} = 0.39 eV) among all the elementary steps, corresponding to the limiting potential (U_L^{urea}) of −0.39 V. Encouragingly, the computed U_L^{urea} value of Mo_2P monolayer is comparable (or even less) to the reported Ru_2B_4 (−0.42 V),[62] Mo_2B_2 (−0.49 V),[31] Pd–Cu catalyst (−0.64 V),[11] and Si-doped C_6N_6 (−0.79 V),[33] indicating its excellent catalytic activity toward urea synthesis.

In addition to the Mo_2P monolayer, we also evaluated the catalytic activity of Ti_2P, Fe_2P, Zr_2P, and W_2P monolayers toward urea formation. Our computational results showed that the *NCON formation on the Fe_2P monolayer by the coupling of $*N_2$ and *CO requires a substantial input energy (0.92 eV, Figure S10, Supporting Information), thus ruling out its capability to further generate urea. As for Ti_2P, Zr_2P,

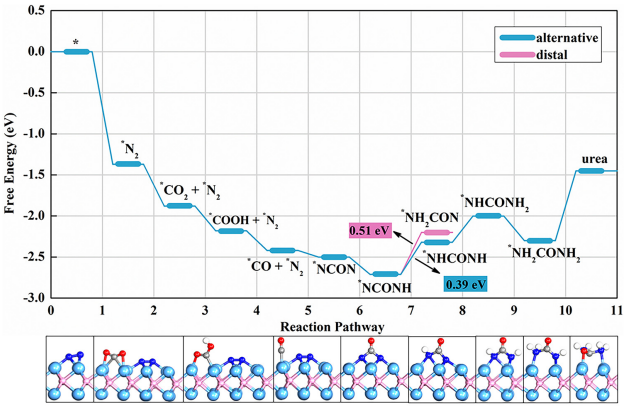

Figure 4. The energetically most favorable free-energy profile for the reduction of N_2 and CO_2 molecules to urea product on the Mo_2P monolayer and the involved reaction intermediates.

and W_2P monolayers, however, the computed U_L^{urea} values are as high as −1.22, −0.91, and −0.90 V (Figure S10, Supporting Information), respectively, which are more negative than the state-of-the-art Pd–Cu catalyst (−0.64 V),[11] suggesting their unsatisfactory catalytic activity for urea production. Thus, only Mo_2P monolayer was screened out as a promising electrocatalyst for urea production.

3.3. Urea Selectivity

In general, NRR, CO_2RR, and HER are regarded as the main competing side reactions of urea synthesis and may result in their low Faraday efficiency.[11] To guarantee the high selectivity toward urea production, the U_L^{urea} should be less negative than the U_L^{NRR}, $U_L^{CO_2RR}$, and U_L^{HER}. Thus, we evaluated the catalytic activity of the Mo_2P monolayer toward NRR, CO_2RR, and HER by computing their free-energy diagrams (Figure S11, Supporting Information).

As revealed by previous reports,[63–73] many Mo-based materials exhibit high NRR activity. On the Mo_2P monolayer, we found that the U_L^{NRR} for N_2 reduction to NH_3 via the most favorable enzymatic mechanism is −0.81 V (Figure S11a, Supporting Information). As for CO_2RR, it is considerably difficult for the hydrogenation of *COOH to *CO due to its large ΔG value of 0.85 eV, corresponding to the $U_L^{CO_2RR}$ of −0.85 V (Figure S11b, Supporting Information). Interestingly, the pre-adsorbed $*N_2$ can activate its adjacent Mo sites, inducing stronger adsorption with *CO species and thus facilitating its further reaction with $*N_2$ to produce the key *NCON precursor. Similarly, HER on Mo_2P monolayer is greatly hindered by the H_2-release due to the high energy input of 0.63 eV (U_L^{HER} = −0.63 V, Figure S11c, Supporting Information). Obviously, the U_L values of these side reactions (−0.81, −0.85, and −0.63 V for NRR, CO_2RR, and HER, respectively) are all more negative than that of urea formation (−0.39 V), which suggests a great suppression effect on these side reactions and thus the high selectivity of the Mo_2P monolayer toward urea production.

3.4. Origin of Excellent Activity of Mo_2P Monolayer for Urea Production

As revealed above, the Mo_2P monolayer exhibits better catalytic activity for urea production than other considered candidates. An interesting question arises naturally: why do these TM_2P-based materials exhibit such a remarkable difference in their catalytic performance for urea formation?

Intrinsically, the activity of a given catalyst is determined by its adsorption strength with reaction intermediates, namely, an ideal catalyst should moderately bind with reaction species according to the Sabatier principle.[74] To this end, we tried to establish a relationship between the catalytic activities (U_L^{urea}) and the adsorption strength of some reaction intermediate. Encouragingly, we obtained a volcano curve between U_L^{urea} and the adsorption energies of *NCON species (ΔE_{*NCON}, **Figure 5**a). Clearly, either too strong (such as Zr_2P and Ti_2P) or too weak (such as Fe_2P) binding strength with *NCON leads to poor catalytic activity for urea production. The optimal ΔE_{*NCON} is about −7.20 eV, where U_L^{urea} is about −0.40 V, corresponding to the Mo_2P monolayer, which is located at the top of the volcano plot. Thus, ΔE_{*NCON} can be utilized as a simple and efficient descriptor to evaluate the catalytic activity for urea synthesis, which may be useful to rapidly predict and further design novel electrocatalysts for urea production.

To unravel the adsorption strength difference between TM_2P monolayers and the *NCON species, we checked the relationship between the charges (Q_{TM}, Table S1, Supporting Information) of these exposed metal active sites and the adsorption energies of *NCON (ΔE_{*NCON}). Interestingly, there is a good linear relationship between ΔE_{*NCON} and Q_{TM} (R^2 = 0.88, Figure 5b), which indicates the moderate adsorption of *NCON species on the Mo_2P monolayer can be ascribed to its moderate positive charges on the exposed Mo active sites. Moreover, we performed the integrated-crystal orbital Hamilton population (ICOHP) analyses of the adsorbed *NCON (Figure S12, Supporting Information) and found that the *NCON adsorption strength is weakened when the anti-bonding orbitals are below E_F. For Zr_2P and Ti_2P, there are few unoccupied anti-bonding orbitals below E_F, while above E_F the orbitals are almost fully occupied by bonding orbitals, thus resulting in strong orbital interaction with *NCON. In particular, there is a linear relationship between ICOHP and ΔE_{*NCON} (Figure 5c), and a more negative ICOHP suggests a stronger adsorption strength. The computed ICOHP values of these candidates are ranging from about −2.05 to −1.09, among which the Mo_2P monolayer has a moderate ICOHP of −1.42, well consistent with its optimal adsorption strength with *NCON to endow its excellent catalytic activity for urea production.

3.5. Feasibility for Experimental Realization and Environment Stability of Mo_2P Monolayer

The aforementioned discussions revealed that the Mo_2P monolayer exhibits superior catalytic performance for urea formation. To explore the feasibility of its experimental synthesis, we compared the formation energy (E_{form}) of the Mo_2P monolayer with those of several experimentally available Mo_xP_y polymorphs using the following equation,

$$E_{form} = \left(E_{Mo_xP_y} - xE_{Mo} - yE_P\right)/(x+y)$$

where $E_{Mo_xP_y}$ is the total energy of one unit cell of Mo_xP_y material, while E_{Mo} and E_P represent the electronic energies of Mo and P atoms, respectively (derived from their stable phases of bulk Mo and P_4 cluster, respectively). According to this definition, lower formation energy indicates higher thermodynamic stability.

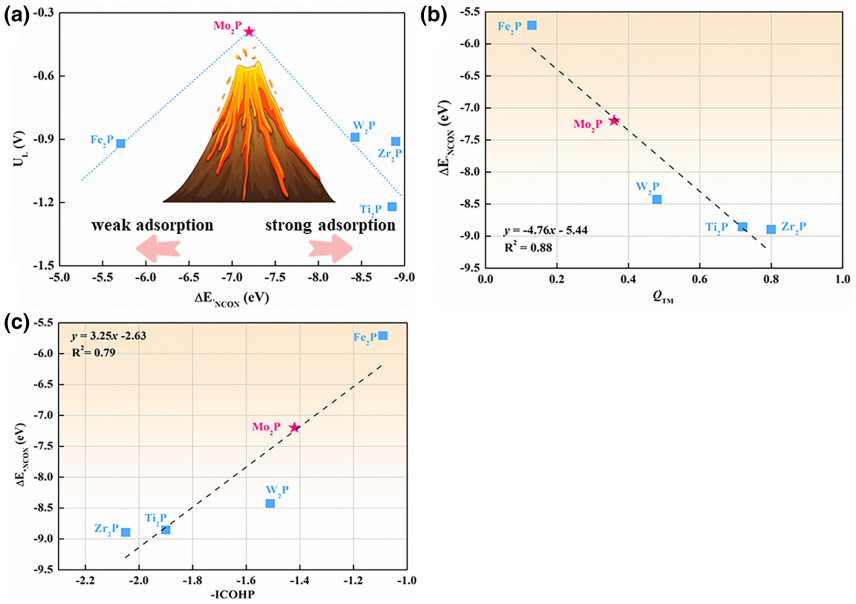

Figure 5. a) Volcano plot of urea formation. Adsorption energy of *NCON (ΔE_{*NCON}) as a function of b) the positive charge on the exposed metal active sites (Q_{TM}, *e*) and c) the integrated-crystal orbital Hamilton population (ICOHP) analyses of adsorbed *NCON (ICOHP).

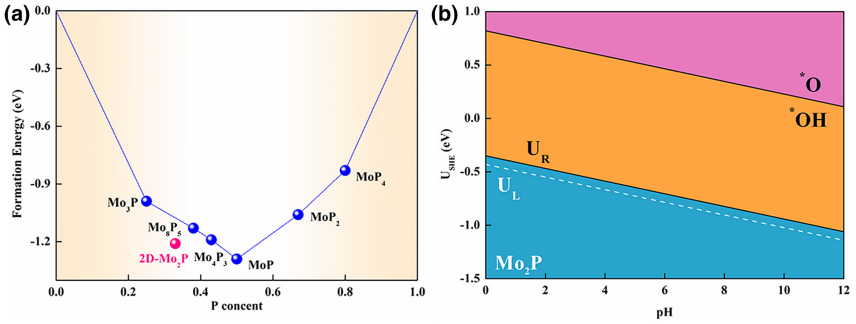

Figure 6. a) The computed relative formation energies (eV) of various Mo_xP_y materials. b) the surface Pourbaix diagrams of Mo_2P.

Amazingly, the computed E_{form} of the Mo_2P monolayer (−1.20 eV) is comparable to (or even lower than) other synthesized Mo_xP_y materials (**Figure 6**a), the Mo_2P monolayer nearly sits on the convex hull (except for MoP), suggesting that the Mo_2P monolayer holds great promise for synthesis under appropriate conditions.

Finally, the environmental stability of the Mo_2P monolayer was assessed by AIMD simulations at 300 K in the water environment. Our results showed that the atomic structure of the Mo_2P monolayer remains intact in the water environment after 5 ps (Figure S13, Supporting Information), as the deviation of Mo–P bond length is <0.05 Å as compared to its equilibrium structure in a vacuum, indicating its high electrochemical stability in aqueous solutions and thus guaranteeing its practical application for urea synthesis under appropriate reaction conditions.

The electrochemical stability is also vital for a given catalyst, and thus we explored the surface Pourbaix diagram of the Mo_2P monolayer to explore its surface structure at different pH and potentials.[31,75] As shown in Figure 6b, when the electrode potential is 0 V, the Mo_2P surface is covered by *OH species regardless of the pH value. However, under applied electrode potential, *OH species will be protonated to H_2O, and the Mo_2P surface will be exposed again. Remarkably, the redox potential (U_R) of the Mo_2P monolayer is less negative than the corresponding U_L, suggesting its superior electrochemical stability under a work potential. In addition, the dissolution potential (U_{diss}) was computed to evaluate the electrochemical stability of the Mo_2P monolayer based on the equation

$$U_{diss} = U^{\circ}_{diss} - \frac{E_f}{ne}$$

where U°_{diss} and *n* represent the standard dissolution potential of bulk metal and the number of electrons involved in the dissolution, respectively, and E_f is the formation energy. The computed U_{diss} value of the Mo_2P monolayer is 0.40 V, suggesting its excellent resistance to dissolution under practical conditions.

Although Mo_2P monolayer was predicted to exhibit superior catalytic performance for urea production, there is no prior study on its experimental synthesis at present. Encouragingly, Feng et al. and Zhou et al. have successfully synthesized 2D Co_2P by the salt-templating method,[20,76] which greatly inspires to fabricate 2D Mo_2P nanosheet through similar experimental strategies. Fortunately, by searching for various salt substrates, we found that the (111) surface of the hexagonal NaCl substrate has a small lattice mismatch (3.50%) with the Mo_2P monolayer (Figure S14, Supporting Information), suggesting that our proposed 2D Mo_2P can be grown on the NaCl surface based on lattice-matching limitation mechanism.[28,77] We hope that our results will inspire more experimental groups to synthesize the Mo_2P monolayer and its analogs.

4. Conclusion

In summary, by means of DFT computations, we explored the potential of several TM_2P monolayers as promising electrocatalysts for urea production. Our results revealed that the Mo_2P monolayer exhibits the best catalytic performance for urea formation due to its intrinsic metallic nature, good stability, small kinetic barrier for C–N coupling (0.35 eV), low limiting potential (−0.39 V), overwhelming suppression on the side reactions, and great promises for experimental synthesis. Remarkably, the optimal adsorption strength of *NCON species on Mo_2P monolayer well illustrates its ultra-high activity toward urea synthesis due to its unique electronic properties. This study not only provides a new way for the fixation of inert N_2 and CO_2 to value-added chemicals, but also further widens the potential application of metal phosphides in electrocatalysis.

5. Experimental Section

Our spin-polarized DFT calculations were performed with the plane-wave basis set as implemented in the Vienna Ab Initio Simulation Package (VASP). The projector augmented wave (PAW) potential was employed to describe the interactions between electrons and ions. The exchange–correlation interactions were determined by the Perdew–Burke–Ernzerhof (PBE) functional within the generalized gradient approximation (GGA), and a cutoff energy of 550 eV was adopted for the plane-wave basis set. The convergence criteria for the residual force and the energy on each atom during structure were set to 0.03 eV $Å^{-1}$ and 10^{-5} eV, respectively. The empirical correction in Grimme's method (DFT+D3) was used to describe the van der Waals (vdW) interactions. The climbing image nudged elastic band (CI–NEB) method was utilized to locate the involved transition states. The adsorption energy (E_{ads}) of adsorbed species on the catalyst surface was defined as $E_{ads} = E_{total} - E_{adsorbate} - E_{catalyst}$, in which E_{total}, $E_{adsorbate}$, and $E_{surface}$ represent the total energies of adsorbed species on the catalyst, isolated adsorbate, and catalyst, respectively. According to this definition, a more negative E_{ads} represents a stronger interaction between adsorbate and catalyst.

TM_2P-based catalysts were built using a 5×5 supercell, in which a vacuum space of 15 Å in the *z*–direction was employed to avoid the interactions between adjacent periodic images. A $3 \times 3 \times 1$ Monkhorst–Pack *k*–point mesh was adopted to sample the 2D Brillouin zone for structure optimizations, while a denser $15 \times 15 \times 1$ *k*–point was used for electronic property computations. The band structures were computed by the Heyd–Scuseria–Ernzerhof (HSE) hybrid functional. Ab initio molecular dynamics (AIMD) simulations using the NVT ensemble were carried out to evaluate the environmental stability of Mo_2P materials. The phonon spectra were computed to assess their kinetic stability based on the density functional perturbation theory (DFPT) using Phonopy code. The change in the Gibbs free energy change (ΔG) for each possible step during the electrochemical synthesis of urea was obtained using the computational hydrogen electrode (CHE) model, and further details on the computations of free energy diagrams and limiting potentials are given in the Supporting Information.

Acknowledgements

D.J. and Z.W. contributed equally to this work. This work was financially supported in China by Natural Science Funds for Distinguished Young Scholars of Heilongjiang Province (No. JC2018004) and Natural Science Foundation of Heilongjiang Province of China (No. TD2020B001), and in the USA by NSF-CREST Center for Innovation, Research, and Education in Environmental Nanotechnology (CIRE2N) (No. HRD-1736093). The authors are very grateful to Prof. Haifeng Wang for helpful suggestions and discussions.

Conflict of Interest

The authors declare no conflict of interest.

Supporting Information

Supporting Information is available from the Wiley Online Library or from the author.

Keywords

C–N coupling, density functional theory, Mo_2P monolayer, urea synthesis

Received: May 29, 2022
Revised: July 3, 2022
Published online: July 18, 2022

[1] J. W. Erisman, M. A. Sutton, J. Galloway, Z. Klimont, W. Winiwarter, *Nat. Geosci.* **2008**, *1*, 636.
[2] C. Chen, N. He, S. Wang, *Small Sci.* **2021**, *1*, 2100070.
[3] Y. Liu, X. Zhao, L. Ye, *Ind. Eng. Chem. Res.* **2016**, *55*, 8743.
[4] C. Lv, L. Zhong, H. Liu, Z. Fang, C. Yan, M. Chen, Y. Kong, C. Lee, D. Liu, S. Li, J. Liu, L. Song, G. Chen, Q. Yan, G. Yu, *Nat. Sustain.* **2021**, *4*, 868.
[5] J. Zheng, L. Jiang, Y. Lyu, S. P. Jiang, S. Wang, *Energy Environ. Mater.* **2022**, *5*, 452.
[6] F. Wang, L. Xia, X. Li, W. Yang, Y. Zhao, J. Mao, *Energy Environ. Mater.* **2021**, *4*, 88.
[7] M. Xia, C. Mao, A. Gu, A. A. Tountas, C. Qiu, T. E. Wood, Y. F. Li, U. Ulmer, Y. Xu, C. J. Viasus, J. Ye, C. Qian, G. Ozin, *Angew. Chem. Int. Ed.* **2022**, *61*, e202110158.
[8] C. Zhu, M. Wang, C. Wen, M. Zhang, Y. Geng, G. Zhu, Z. Su, *Adv. Sci.* **2022**, *9*, 2105697.
[9] C. Lv, C. Lee, L. Zhong, H. Liu, J. Liu, L. Yang, C. Yan, W. Yu, H. H. Hng, Z. Qi, L. Song, S. Li, K. P. Loh, Q. Yan, G. Yu, *ACS Nano* **2022**, *16*, 8213.
[10] J. Li, J. Li, T. Liu, L. Chen, Y. Li, H. Wang, X. Chen, M. Gong, Z.-P. Liu, X. Yang, *Angew. Chem. Int. Ed.* **2021**, *60*, 26656.
[11] C. Chen, X. Zhu, X. Wen, Y. Zhou, L. Zhou, H. Li, L. Tao, Q. Li, S. Du, T. Liu, D. Yan, C. Xie, Y. Zou, Y. Wang, R. Chen, J. Huo, Y. Li, J. Cheng, H. Su, X. Zhao, W. Cheng, Q. Liu, H. Lin, J. Luo, J. Chen, M. Dong, K. Cheng, C. Li, S. Wang, *Nat. Chem.* **2020**, *12*, 717.
[12] M. Yuan, J. Chen, Y. Bai, Z. Liu, J. Zhang, T. Zhao, Q. Shi, S. Li, X. Wang, G. Zhang, *Chem. Sci.* **2021**, *12*, 6048.
[13] M. Yuan, J. Chen, Y. Bai, Z. Liu, J. Zhang, T. Zhao, Q. Wang, S. Li, H. He, G. Zhang, *Angew. Chem. Int. Ed.* **2021**, *60*, 10910.
[14] M. Yuan, H. Zhang, Y. Xu, R. Liu, R. Wang, T. Zhao, J. Zhang, Z. Liu, H. He, C. Yang, S. Zhang, G. Zhang, *Chem Catal.* **2022**, *2*, 309.
[15] M. Yuan, J. Chen, Y. Xu, R. Liu, T. Zhao, J. Zhang, Z. Ren, Z. Liu, C. Streb, H. He, C. Yang, S. Zhang, G. Zhang, *Energy Environ. Sci.* **2021**, *14*, 6605.
[16] H. Jin, C. Guo, X. Liu, J. Liu, A. Vasileff, Y. Jiao, Y. Zheng, S.-Z. Qiao, *Chem. Rev.* **2018**, *118*, 6337.
[17] J. Zhu, S. Li, Z. Zhuang, S. Gao, X. Hong, X. Pan, R. Yu, L. Zhou, L. V. Moskaleva, L. Mai, *Energy Environ. Mater.* **2022**, *5*, 231.
[18] X. Chia, M. Pumera, *Nat. Catal.* **2018**, *1*, 909.
[19] Z. Liu, T. Huang, H. Chang, F. Wang, J. Wen, H. Sun, M. Hossain, Q. Xie, Y. Zhao, Y. Wu, *Energy Environ. Mater.* **2021**, *4*, 255.
[20] S. Yang, G. Chen, A. G. Ricciardulli, P. Zhang, Z. Zhang, H. Shi, J. Ma, J. Zhang, P. W. M. Blom, X. Feng, *Angew. Chem. Int. Ed.* **2020**, *59*, 465.
[21] Z. Pu, T. Liu, I. S. Amiinu, R. Cheng, P. Wang, C. Zhang, P. Ji, W. Hu, J. Liu, S. Mu, *Adv. Funct. Mater.* **2020**, *30*, 2004009.
[22] Y. Shi, M. Li, Y. Yu, B. Zhang, *Energy Environ. Sci.* **2020**, *13*, 4564.
[23] X. Zhao, X. Kong, Z. Liu, Z. Li, Z. Xie, Z. Wu, F. He, X. Chang, P. Yang, J. Zheng, X. Li, *Nano Today* **2021**, *40*, 101245.
[24] S. Wang, G. Li, L. Chen, Z. Li, Z. Wu, X. Kong, T. Wang, F. He, P. Yang, Z. Liu, *Funct. Mater. Lett.* **2021**, *14*, 2130017.
[25] W. Zhu, C. Tang, D. Liu, J. Wang, A. M. Asiri, X. Sun, *J. Mater. Chem. A* **2016**, *4*, 7169.
[26] H. Lou, K. Qiu, G. Yang, *ACS Appl. Mater. Inter.* **2021**, *13*, 57422.
[27] Y. Sun, S. Wang, D. Jiao, F. Li, S. Qiu, Z. Wang, Q. Cai, J. Zhao, C. Sun, *Chinese Chem. Lett.* **2022**, *33*, 3987.
[28] Q. Liu, J. Xing, Z. Jiang, X. Jiang, Y. Wang, J. Zhao, *Nanoscale* **2020**, *12*, 6776.
[29] J. Wu, J.-H. Li, Y.-X. Yu, *Sci. Technol.* **2021**, *11*, 1419.
[30] S. Zheng, T. Yu, J. Lin, H. Lou, H. Xu, G. Yang, *J. Mater. Chem. A* **2019**, *7*, 25665.
[31] X. Zhu, X. Zhou, Y. Jing, Y. Li, *Nat. Commun.* **2021**, *12*, 4080.
[32] C. Zhu, C. Wen, M. Wang, M. Zhang, Y. Geng, Z. Su, *Chem. Sci.* **2022**, *13*, 1342.
[33] P. Roy, A. Pramanik, P. Sarkar, *J. Phys. Chem. Lett.* **2021**, *12*, 10837.
[34] G. Kresse, J. Hafner, *Phys. Rev. B* **1993**, *47*, 558.

[35] G. Kresse, J. Furthmüller, *Phys. Rev. B* **1996**, *54*, 11169.
[36] P. E. Blöchl, *Phys. Rev. B* **1994**, *50*, 17953.
[37] G. Kresse, D. Joubert, *Phys. Rev. B* **1999**, *59*, 1758.
[38] J. P. Perdew, K. Burke, M. Ernzerhof, *Phys. Rev. Lett.* **1996**, *77*, 3865.
[39] S. Grimme, *J. Comput. Chem.* **2006**, *27*, 1787.
[40] G. Henkelman, B. P. Uberuaga, H. Jónsson, *J. Chem. Phys.* **2000**, *113*, 9901.
[41] J. Heyd, G. E. Scuseria, M. Ernzerhof, *J. Chem. Phys.* **2003**, *118*, 8207.
[42] J. Paier, M. Marsman, K. Hummer, G. Kresse, I. C. Gerber, J. G. Ángyán, *J. Chem. Phys.* **2006**, *124*, 154709.
[43] G. J. Martyna, M. L. Klein, M. Tuckerman, *J. Chem. Phys.* **1992**, *97*, 2635.
[44] X. Gonze, C. Lee, *Phys. Rev. B* **1997**, *55*, 10355.
[45] J. K. Nørskov, J. Rossmeisl, A. Logadottir, L. Lindqvist, J. R. Kitchin, T. Bligaard, H. Jónsson, *J. Phys. Chem. B* **2004**, *108*, 17886.
[46] A. A. Peterson, F. Abild-Pedersen, F. Studt, J. Rossmeisl, J. K. Nørskov, *Energy Environ. Sci.* **2010**, *3*, 1311.
[47] Y. Shao, X. Shi, H. Pan, *Chem. Mater.* **2017**, *29*, 8892.
[48] Z. Cheng, X. Zhang, H. Zhang, H. Liu, X. Yu, X. Dai, G. Liu, G. Chen, *Phys. Chem. Chem. Phys.* **2020**, *22*, 18480.
[49] X. Liu, S. Lin, J. Gao, H. Shi, S.-G. Kim, Z. Chen, H. Lee, *Phys. Chem. Chem. Phys.* **2021**, *23*, 4030.
[50] J. Wu, J. Wen, Y.-X. Yu, *Appl. Surf. Sci.* **2021**, *565*, 150567.
[51] J. Guan, Z. Zhu, D. Tománek, *Phys. Rev. Lett.* **2014**, *113*, 046804.
[52] Y. Zhao, Q. Liu, J. Xing, X. Jiang, J. Zhao, *Nanoscale Adv.* **2022**, *4*, 600.
[53] J. Wang, S. Yip, S. R. Phillpot, D. Wolf, *Phys. Rev. Lett.* **1993**, *71*, 4182.
[54] X. Lv, W. Wei, P. Zhao, D. Er, B. Huang, Y. Dai, T. Jacob, *J. Catal.* **2019**, *378*, 97.
[55] X. Huang, J. Wang, H. Bing Tao, H. Tian, Z. Zhang, H. Xu, *J. Catal.* **2020**, *389*, 461.
[56] J. Zhang, J. Wu, H. Guo, W. Chen, J. Yuan, U. Martinez, G. Gupta, A. Mohite, P. M. Ajayan, J. Lou, *Adv. Mater.* **2017**, *29*, 1701955.
[57] Y. Li, H. Su, S. H. Chan, Q. Sun, *ACS Catal.* **2015**, *5*, 6658.
[58] J. Mukherjee, S. Paul, A. Adalder, S. Kapse, R. Thapa, S. Mandal, B. Ghorai, S. Sarkar, U. K. Ghorai, *Adv. Funct. Mater.* **2022**, *32*, 2200882.
[59] K. Mathew, R. Sundararaman, K. Letchworth-Weaver, T. A. Arias, R. G. Hennig, *J. Chem. Phys.* **2014**, *140*, 084106.
[60] J. Long, C. Guo, X. Fu, H. Jing, G. Qin, H. Li, J. Xiao, *J. Phys. Chem. Lett.* **2021**, *12*, 6988.
[61] X. Huang, L.-Y. Gan, J. Wang, S. Ali, C.-C. He, H. Xu, *J. Phys. Chem. Lett.* **2021**, *12*, 9197.
[62] Y. Xiao, C. Shen, Z. Xiong, J. Li, W. Zhang, *Mater. Today Phys.* **2022**, *26*, 100726.
[63] J. Zhao, Z. Chen, *J. Am. Chem. Soc.* **2017**, *139*, 12480.
[64] C. Wang, Y.-T. Shan, W.-H. Zheng, M. Zhang, Z.-M. Su, *Appl. Surf. Sci.* **2022**, *580*, 152359.
[65] L. Zhang, X. Ji, X. Ren, Y. Ma, X. Shi, Z. Tian, A. M. Asiri, L. Chen, B. Tang, X. Sun, *Adv. Mater.* **2018**, *30*, 1800191.
[66] Y. Ma, T. Yang, H. Zou, W. Zang, Z. Kou, L. Mao, Y. Feng, L. Shen, S. J. Pennycook, L. Duan, X. Li, J. Wang, *Adv. Mater.* **2020**, *32*, 2002177.
[67] V. Yandulov Dmitry, R. Schrock Richard, *Science* **2003**, *301*, 76.
[68] S. Lv, C. Huang, G. Li, L. Yang, *Energy Environ. Mater.* **2022**, *5*, 533.
[69] H. Cheng, L.-X. Ding, G.-F. Chen, L. Zhang, J. Xue, H. Wang, *Adv. Mater.* **2018**, *30*, 1803694.
[70] L. Han, X. Liu, J. Chen, R. Lin, H. Liu, F. Lü, S. Bak, Z. Liang, S. Zhao, E. Stavitski, J. Luo, R. R. Adzic, H. L. Xin, *Angew. Chem. Int. Ed.* **2019**, *58*, 2321.
[71] C. Ling, X. Bai, Y. Ouyang, A. Du, J. Wang, *J. Phys. Chem. C* **2018**, *122*, 16842.
[72] K. Chu, Y.-P. Liu, Y.-B. Li, Y.-L. Guo, Y. Tian, H. Zhang, *Appl. Catal. B Environ.* **2020**, *264*, 118525.
[73] Z. W. Chen, X. Y. Lang, Q. Jiang, *J. Mater. Chem. A* **2018**, *6*, 9623.
[74] A. J. Medford, A. Vojvodic, J. S. Hummelshøj, J. Voss, F. Abild-Pedersen, F. Studt, T. Bligaard, A. Nilsson, J. K. Nørskov, *J. Catal.* **2015**, *328*, 36.
[75] X. Guo, S. Lin, J. Gu, S. Zhang, Z. Chen, S. Huang, *Adv. Funct. Mater.* **2021**, *31*, 2008056.
[76] T. Li, H. Jin, Z. Liang, L. Huang, Y. Lu, H. Yu, Z. Hu, J. Wu, B. Y. Xia, G. Feng, J. Zhou, *Nanoscale* **2018**, *10*, 6844.
[77] X. Xiao, H. Song, S. Lin, Y. Zhou, X. Zhan, Z. Hu, Q. Zhang, J. Sun, B. Yang, T. Li, L. Jiao, J. Zhou, J. Tang, Y. Gogotsi, *Nat. Commun.* **2016**, *7*, 11296.